

# Automated Seismic Source Characterisation Using Deep Graph Neural Networks

M. P. A. van den Ende<sup>1</sup>, J.-P. Ampuero<sup>1</sup>

<sup>1</sup>Université Côte d'Azur, IRD, CNRS, Observatoire de la Côte d'Azur, Géoazur, France

## Key Points:

- We propose a deep learning approach for automated earthquake location and magnitude estimation based on Graph Neural Network theory
- This new approach processes multi-station waveforms and incorporates station locations explicitly
- Including station locations improves the accuracy of epicentre estimation compared to models that are location-agnostic

---

Corresponding author: M. P. A. van den Ende, [martijn.vandenende@geoazur.unice.fr](mailto:martijn.vandenende@geoazur.unice.fr)

**12 Abstract**

13 Most seismological analysis methods require knowledge of the geographic location of the  
14 stations comprising a seismic network. However, common machine learning tools used  
15 in seismology do not account for this spatial information, and so there is an underutilised  
16 potential for improving the performance of machine learning models. In this work, we  
17 propose a Graph Neural Network (GNN) approach that explicitly incorporates and lever-  
18 ages spatial information for the task of seismic source characterisation (specifically, lo-  
19 cation and magnitude estimation), based on multi-station waveform recordings. Even  
20 using a modestly-sized GNN, we achieve model prediction accuracy that outperforms meth-  
21 ods that are agnostic to station locations. Moreover, the proposed method is flexible to  
22 the number of seismic stations included in the analysis, and is invariant to the order in  
23 which the stations are arranged, which opens up new applications in the automation of  
24 seismological tasks and in earthquake early warning systems.

**25 Plain language summary**

26 To determine the location and size of earthquakes, seismologists use the geographic  
27 locations of the seismic stations that record the ground shaking in their data analysis  
28 workflow. By taking the distance between stations and the relative timing of the onset  
29 of the shaking, the origin of the seismic waves can be accurately reconstructed. In re-  
30 cent years, machine learning (a subfield of artificial intelligence) has shown great poten-  
31 tial to automate seismological tasks, such as earthquake source localisation. Most ma-  
32 chine learning methods do not take into consideration the geographic locations of the  
33 seismic stations, and so the usefulness of these methods could still be improved by pro-  
34 viding the locations at which the data was recorded. In this work, we propose a method  
35 that accounts for geographic locations of the seismic stations, and we show that this im-  
36 proves the machine learning predictions.

**37 1 Introduction**

38 Seismic source characterisation is a primary task in earthquake seismology, and in-  
39 volves the estimation of the epicentral location, hypocentral depth, and seismic moment  
40 of earthquakes. Particularly for the purposes of earthquake early warning, emergency  
41 response and timely information dissemination, an estimate of the seismic source char-  
42 acteristics needs to be produced rapidly, preferably without the intervention of an an-

43 alyst. One computational tool that satisfies these requirements is machine learning, mak-  
44 ing it a potential candidate to address the challenge of rapid seismic source character-  
45 isation.

46 Recently, attempts have been made to apply machine learning to seismic source  
47 characterisation (Perol et al., 2018; Lomax et al., 2019; Kriegerowski et al., 2019; Mousavi  
48 & Beroza, 2020). In the ConvNetQuake approach of Perol et al. (2018), a convolutional  
49 neural network was adopted to distinguish between noise and earthquake waveforms, and  
50 to determine the regional earthquake cluster from which each event originated. This method  
51 was extended by Lomax et al. (2019) to global seismicity. Mousavi & Beroza (2020) em-  
52 ployed a combined convolutional-recurrent neural network to estimate earthquake mag-  
53 nitudes. It is noteworthy that these methods only accept single-station waveforms as an  
54 input, which goes against the common intuition that at least three seismic stations are  
55 required to triangulate and locate a seismic source. One possible explanation for the per-  
56 formance of these methods is that they rely on waveform similarity (Perol et al., 2018)  
57 and differences in phase arrival times (Mousavi & Beroza, 2020). Unfortunately, owing  
58 to the opacity of the methods, this hypothesis is not easily tested.

59 Alternatively, a multi-station approach would take as input for each earthquake all  
60 the waveforms recorded by the seismic network. One compelling argument in favor of  
61 single-station approaches is that for each earthquake there are as many training sam-  
62 ples as there are stations, whereas in the multi-station approach there is only one train-  
63 ing sample per earthquake (the concatenated waveforms from the whole network). Since  
64 the performance of a deep learning model scales with the volume of data available for  
65 training, the model predictions may not improve when combining multiple station data  
66 into a single training sample. Moreover, concatenating data from multiple stations in a  
67 meaningful way is non-trivial. If the seismic network has a Euclidean structure, i.e. if  
68 it is arranged in a regular pattern like for uniformly-spaced seismic arrays or fibre-optic  
69 distributed acoustic sensing, the data can be naturally arranged into e.g. a 2D image,  
70 where the distance between each pixel is representative of the spatial sampling distance.  
71 Unfortunately, most seismic networks are not arranged in a regular structure, so that  
72 the geometry of the network needs to be learned implicitly, as was attempted by Kriegerowski  
73 et al. (2019). Even though this approach yielded acceptable hypocentre location estimates,  
74 it remains an open question whether better results could be achieved when the non-Euclidean  
75 nature of the seismic network is better accounted for. Moreover, the seismic stations com-

prising the network may not be continuously operational over the period of interest (due to (de)commissioning, maintenance, or temporary campaigning strategies), leading to gaps in the fixed Euclidean data structure. Rather, seismic networks are better represented by a time-varying *graph* structure.

The deep learning tools most commonly used in seismology, convolutional neural networks (CNNs) and multi-layer perceptrons (MLPs), are well suited to Euclidean data structures, but are not optimal for graph data structures. One important characteristic of graphs is that they are not defined by the ordering or positioning of the data, but only by the relations between data. As such, valid operations on a graph need to be invariant to the data order. This is not generally the case for CNNs, which exploit ordering as a proxy for spatial distance, nor for MLPs, which rely on the constant structure of the input features. Fortunately, much progress has been made in the field of *Graph Neural Networks* (GNNs; Gori et al., 2005; Zhou et al., 2019), providing a robust framework for analysing non-Euclidean data using existing deep learning tools.

In this contribution, we will demonstrate how GNNs can be applied to seismic source characterisation using data from multiple seismic stations simultaneously. The method does not require a fixed seismic network configuration, and so the number of stations to be included in each sample is allowed to vary over time. Moreover, the stations do not need to be ordered geographically or as a function of distance from the seismic source. This makes the proposed method suitable for earthquake early warning and disaster response applications, in which the number and location of stations on which a given event is recorded is not known a-priori.

## 2 Methods

### 2.1 Basic Concepts of Graph Neural Networks

Over the past several years, numerous deep learning techniques have been proposed that allow for the analysis of non-Euclidean data structures (Bronstein et al., 2017; Zhou et al., 2019), which has found applications in point cloud data (Qi et al., 2017; Wang et al., 2019), curved manifolds (Monti et al., 2017), and  $N$ -body classical mechanics (Sanchez-Gonzalez et al., 2019), among many others. As a subclass of non-Euclidean objects, graphs highlight relations between objects, typically represented as nodes connected by edges. Commonly studied examples of graph-representable objects include social networks (Hamil-

107 ton et al., 2017), molecules (Duvenaud et al., 2015), and urban infrastructures (Cui et  
 108 al., 2019). Owing to the lack of spatial ordering of graph structures, mathematical op-  
 109 erations performed on graphs need to be invariant to the order in which the operations  
 110 are executed. Moreover, nodes and relations between them (i.e. the edges) may not be  
 111 fixed, and so the graph operations need to generalise to an arbitrary number of nodes  
 112 and/or edges (and potentially the number of graphs) at any given moment. In essence,  
 113 suitable graph operations are those that can be applied to the elements of a *set* of un-  
 114 known cardinality. These can be simple mathematical operations such as taking the mean,  
 115 maximum, or sum of the set, or they can involve more expressive aggregation (Battaglia  
 116 et al., 2018) and message passing (Gilmer et al., 2017) operations.

117 To make the above statement more concrete, we represent a seismic network by an  
 118 edgeless graph in which each seismic station is a node. For the task of seismic source char-  
 119 acterisation, the relations between individual stations are not physically meaningful, and  
 120 so we do not include edges connecting the nodes in the analysis, reducing the graph to  
 121 an unordered set. While a graph with no edges may seem ludicrous, the existence of edges  
 122 is not a requirement for defining a graph, and basic architectural principles (e.g. Battaglia  
 123 et al., 2018) still apply. Naturally, in cases where the relation between stations is rele-  
 124 vant, edge information should be included. Each node in our graph carries two attributes:  
 125 a three-component seismic waveform time-series, and a geographic location. The graph  
 126 itself carries four attributes: the latitude, longitude, depth, and magnitude of the seis-  
 127 mic source. Through suitable processing and aggregation of the node attributes, the ob-  
 128 jective for the GNN is to predict the graph attributes.

## 129 2.2 Model architecture

130 The model architecture employed in this work consists of three components that  
 131 operate sequentially – see Fig. 1 and Supplementary Text S1 for details (Tompson et al.,  
 132 2015; Saxe et al., 2014; Hu et al., 2020). Firstly, we analyse the waveforms of a given sta-  
 133 tion using a CNN. This CNN processes the three-component waveform (comprising  $N_t$   
 134 time samples) and extracts a set of  $N_f$  features. The geographic location (latitude/longitude)  
 135 of the seismic station is then appended to produce a feature vector of size  $N_f+2$ . This  
 136 feature vector serves as an input for the second component: an MLP that recombines  
 137 the time-series features and station location into a final station-specific feature vector  
 138 of size  $N_q$ . This process is repeated for all  $N_s$  stations in the network using the same CNN

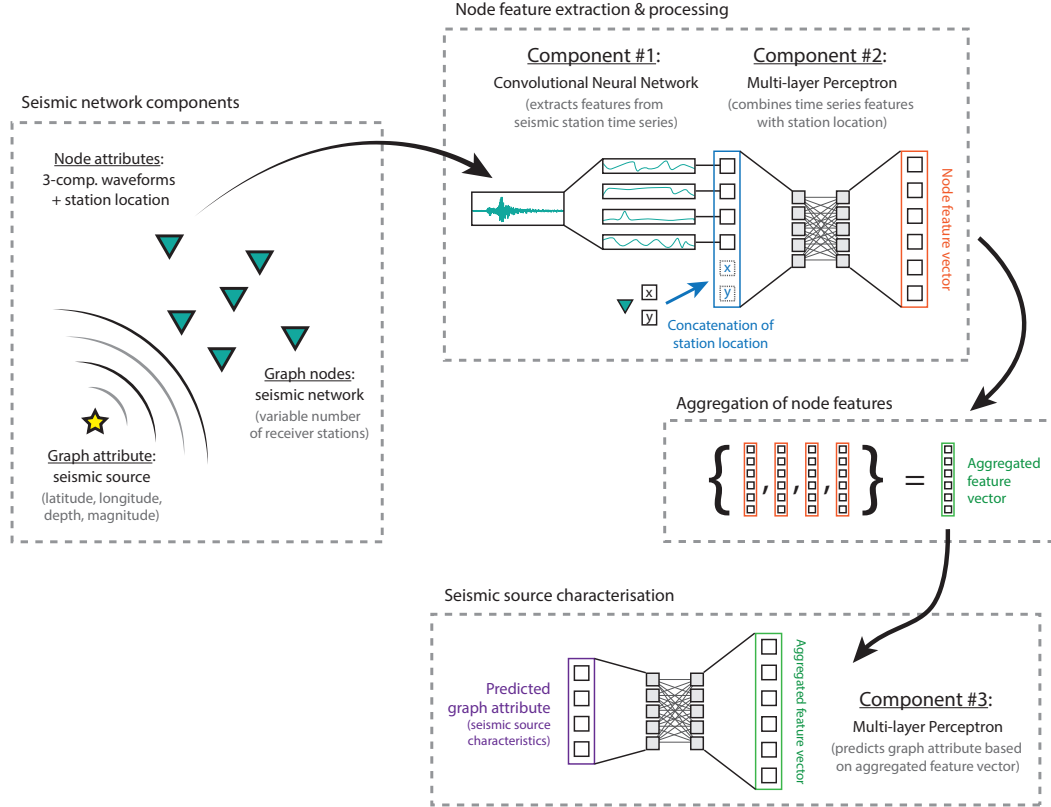


**Figure 1.** Synoptic overview of the adopted model architecture. The three-component waveforms from a receiver station are fed into a CNN, after which the extracted features are combined with the station’s geographic location and further processed by an MLP. The resulting node feature vector of all the stations are aggregated, and this aggregated feature vector is passed through a second MLP that predicts the seismic source characteristics.

139 and MLP components (i.e. the exact same operations are applied to each station indi-  
 140 dually). The convolution operations are performed only along the time axis. The out-  
 141 put of the CNN after concatenation with each station location is then of size  $N_s \times (N_f + 2)$ ,  
 142 and the output of the MLP is of size  $N_s \times N_q$ .

143 After processing of the node attributes (the waveforms and locations of each sta-  
 144 tion), the output of the MLP is max reduced over all stations to yield a graph feature  
 145 vector. Empirically we have found that a max reduce yields better results than averag-  
 146 ing or summation. The extracted features carry no physical meaning, and the informa-  
 147 tion content of the feature vectors adapts to the type of aggregation during training. Hence,  
 148 the most suitable type of aggregation needs to be determined experimentally. Finally,

149 the graph feature vector is fed into a second MLP to predict the graph attributes, be-  
150 ing the latitude, longitude, depth, and magnitude of the seismic source. Each of these  
151 source attributes is scaled so that they fall within the continuous range of  $-1 < x <$   
152  $+1$ , enforced by a tanh activation function in the last layer in the network. In contrast  
153 to previous work (Perol et al., 2018; Lomax et al., 2019), no binning of the source char-  
154 acteristics is performed. Moreover, we do not perform event detection, as this has already  
155 been done in numerous previous studies (Dysart & Pulli, 1990; Li et al., 2018; Mousavi  
156 et al., 2019; Wu et al., 2019, and others) and is essentially a solved problem. Instead,  
157 we focus on the characterisation of a given seismic event. Note that the procedure above  
158 is intrinsically invariant to the number and ordering of the seismic stations: the feature  
159 extraction and re-combination with the geographic location is performed for each node  
160 individually and does not incorporate information from the neighbouring stations. The  
161 aggregation and the resulting graph feature vector are also independent of the number  
162 and ordering of stations. Finally, the seismic source characteristics are predicted from  
163 this invariant graph feature vector, and are hence completely independent of the network  
164 input ordering and size.

165 To regularise the learning process, we include dropout regularisation (Srivastava  
166 et al., 2014) with a dropout rate of 15 % between each layer in each model component.  
167 Since the mechanics of convolutional layers are different from “dense” layers (those defin-  
168 ing the MLPs), we use *spatial dropout* regularisation (Tompson et al., 2015) that ran-  
169 domly sets entire feature maps of a convolutional layer to zero (as opposed to individ-  
170 ual elements in the feature maps). The use of dropout regularisation is dually motivated:  
171 first of all it reduces overfitting on the training set, as the model cannot rely on a sin-  
172 gular layer output (which could be randomly set to zero), promoting redundancy and gen-  
173 eralisation within the model. Secondly, by randomly perturbing the data flow within the  
174 neural networks, the model output becomes probabilistic. The probability distribution  
175 of the model predictions for a given event can be acquired by evaluating a given input  
176 multiple times at inference time. This technique is commonly referred to as Bayesian dropout  
177 (Gal & Ghahramani, 2016), as it yields a posterior distribution and hence provides a means  
178 to estimate the model uncertainty for the predictions.

### 179           **2.3 Data description and training procedure**

180           To construct a training set, we use ObsPy (Beyreuther et al., 2010) to download  
181 the broadband station inventory and earthquake catalogue of the Southern California  
182 Seismic Network (SCSN; Hutton et al., 2010) over the period 2000-2015. For both the  
183 seismic station and event locations, we limit the latitude range from  $32^\circ$  to  $36^\circ$ , and the  
184 longitude range from  $-120^\circ$  to  $-116^\circ$ . The lower earthquake magnitude limit is set to  
185 3 with no depth cut-off. In total, 1377 events and 187 stations are included in the data  
186 set. After downloading the three-component waveforms and removing the instrument  
187 response, we filter the waveforms to a 0.1-8 Hz bandpass and interpolate onto a common  
188 time base of  $1 \leq t \leq 101$  seconds after the event origin time, over 2048 evenly spaced  
189 time samples ( $\approx 20$  Hz sampling frequency). For an average P-wave speed of  $6 \text{ km s}^{-1}$ ,  
190 this time interval allows the stations at the far ends of the domain (roughly  $440 \times 440$   
191 km in size) to record the event while keeping the data volume compact. The lower limit  
192 of the frequency band is chosen below the corner frequency of the earthquakes in this  
193 analysis ( $M_w < 6$ , with corresponding corner frequency  $f_c > 0.2$  Hz; Madariaga, 1976)  
194 such that information regarding the seismic moment is retained. The upper frequency  
195 limit acknowledges the common notion that attenuation and scattering rapidly reduce  
196 the signal spectrum at higher frequencies. Although the start time of all selected wave-  
197 forms is fixed relative to their event origin time, the shift-equivariance of the convolu-  
198 tion layers ensures that the extracted features are not sensitive to their timing with re-  
199 spect to the origin. Subsequent aggregation over the time-axis renders the features strictly  
200 time-invariant. As a result, selecting a different start of the data time window (which  
201 is inevitable when the event origin time is unknown) does not affect the model perfor-  
202 mance. The processed waveforms are stored in a database which includes the locations  
203 of the seismic stations that have recorded the events. Note that not all stations are op-  
204 erational at the time of a given event, and hence the number of stations with recordings  
205 of the event varies.

206           After processing the waveforms, the locations of the stations and seismic source are  
207 scaled by the minimum and maximum latitude/longitude, so that the re-scaled locations  
208 fall in the range of  $\pm 1$ . Such normalisation is generally considered good practice in deep  
209 learning. Similarly, the source depth is scaled to fall in the same range by taking a min-  
210 imum and maximum source depth of 0 and 30 km respectively. The earthquake magni-  
211 tude is scaled taking a minimum and maximum of 3 and 6. The full data set is then ran-



212 domly split 80-20 into a training set and a validation set, respectively. A batch of train-  
213 ing samples is generated on the fly between training epochs by randomly selecting 16 train-  
214 ing events, and 50 randomly selected stations associated with each event, which we con-  
215 sider to strike a good balance between data volume and memory consumption. When  
216 a given event was recorded by fewer than 50 stations, the absent recordings are replaced  
217 by zeros (which do not contribute to the model performance). The model performance  
218 is evaluated through a mean absolute error loss between the predicted and target seis-  
219 mic source characteristics (scaled between  $\pm 1$ ), and training is performed by minimisa-  
220 tion of the loss using the ADAM algorithm (Kingma & Ba, 2017). Training is contin-  
221 ued for 500 epochs, at which point the model performance has saturated. On a single  
222 nVidia Tesla K80, the training phase took about 1 hour in total. Once trained, evalu-  
223 ation of 1377 events with up to 50 stations each takes less than 5 s of computation time  
224 (including data transfer overhead), or 3.5 ms per event.

### 225 **3 Results and Discussion**

#### 226 **3.1 Reference model performance**

227 We evaluate the performance of the trained model on both the training and val-  
228 idation data sets separately (Fig. 2a-d and Supplementary Figure S1). The model pos-  
229 terior is estimated by maintaining dropout regularisation at inference time (as discussed  
230 in the previous section), and performing the inference 100 times on each event in the train-  
231 ing and validation catalogues and calculating the corresponding mean and standard de-  
232 viation. Overall, the performance is similar for either data set, which indicates that over-  
233 fitting on the training set is minimal. The mean absolute difference between the cata-  
234 logue values and the model predictions is less than  $0.11^\circ$  ( $\approx 13$  km in distance) for the  
235 latitude and longitude, 3.3 km for the depth, and 0.13 for the event magnitude. While  
236 these predictions are not as precise as typical non-relocated estimates for Southern Cal-  
237 ifornia (Powers & Jordan, 2010), they are obtained without phase picking, crustal ve-  
238 locity models, nor waveform amplitude modelling. Hence, the method provides a rea-  
239 sonable first-order estimate of location and magnitude that can serve as a starting point  
240 for subsequent refinement based on traditional seismological tools.

241 Since we can compute the posterior distribution for each event, we can compare  
242 the confidence intervals given by the posterior with the true epicentre location error. In

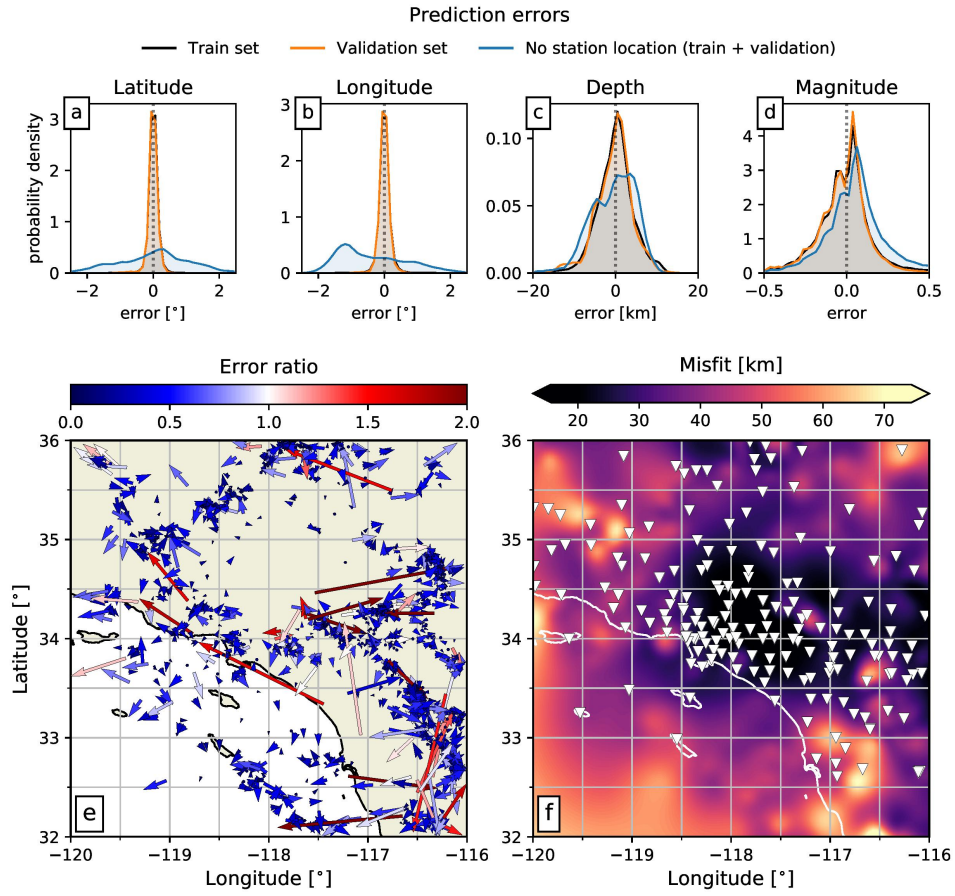


**Figure 2.** (a)-(d) Prediction error distributions for the trained model, for (a) latitude, (b) longitude, (c) depth, and (d) magnitude of each event. The model performance when including the station geographic locations is evaluated separately for the train and validation data sets, showing minimal overfitting. When the station locations are omitted, the performance is evaluated on the combined data set; (e) Residuals of the epicentral locations. Each arrow represents one catalogued event, starting at the predicted epicentre and pointing towards the catalogue epicentre. The colours indicate the ratio of the misfit over the 95 % confidence interval of the model posterior. Hence, blue colours indicate that the catalogue epicentre falls within the 95 % confidence interval, and red colours that the epicentre falls outside of it; (f) Overlay of the locations of seismic stations on the interpolated prediction error (in km)

243 Fig. 2e, we plot the residual vectors between the predicted epicentre locations and those  
244 in the catalogue. To visualise the model uncertainty, we compute an error ratio metric  
245 as the distance between the predicted and catalogued epicentres, normalised by the 95 %  
246 confidence interval obtained from the model posterior. Hence, values less than 1 indi-  
247 cate that the true epicentre location falls within the 95 % confidence interval, while val-  
248 ues greater than 1 indicate the converse. The spatially interpolated prediction error seems  
249 partly correlated with the local density of seismic stations (Fig. 2f), as regions with the  
250 highest station density also exhibit a low prediction error. The largest systematic errors  
251 are found in the northwest and southeast corners of the selected domain, where the sta-  
252 tion density is low and where the model seems unable to achieve the bounding values  
253 of latitude and longitude. This observation can be explained by the behaviour of the tanh  
254 activation function, which asymptotically approaches its range of  $\pm 1$ , corresponding with  
255 the range of latitudes and longitudes of the training samples. Hence, increasingly larger  
256 activations are required to push the final location predictions towards the boundaries of  
257 the domain, biasing the results towards the interior. This highlights a fundamental trade-  
258 off between resolution (prediction accuracy) in the interior of the data domain, and the  
259 maximum amplitude of the predictions (which also applies to linear activation functions).

### 260 **3.2 Importance of a seismic network**

261 A direct test to assess whether the station geographic location information is ac-  
262 tually used in making the predictions (and therefore holds predictive value), we perform  
263 inference on the full data set, but set the station coordinates to a fixed mean value of  
264  $(34^\circ, -118^\circ)$  – see Fig. 2a-d and Supplementary Figure S2. While the predictions for the  
265 event magnitude remain mostly unchanged, the estimation of the epicentre location de-  
266 teriorates and becomes broadly distributed (typical for random predictions). This clearly  
267 indicates that the station location information plays an important role in estimating the  
268 epicentre locations. Thus, the adopted GNN approach, in which station location infor-  
269 mation is provided explicitly, holds an advantage over station-location agnostic meth-  
270 ods. Interestingly, the event magnitude is almost as well resolved as when the station  
271 coordinates are included, which suggests that the model relies on the waveform data but  
272 not on station locations to estimate the magnitude. This was also observed by Mousavi  
273 & Beroza (2020), who proposed that the relative timing of the P- and S-wave arrivals

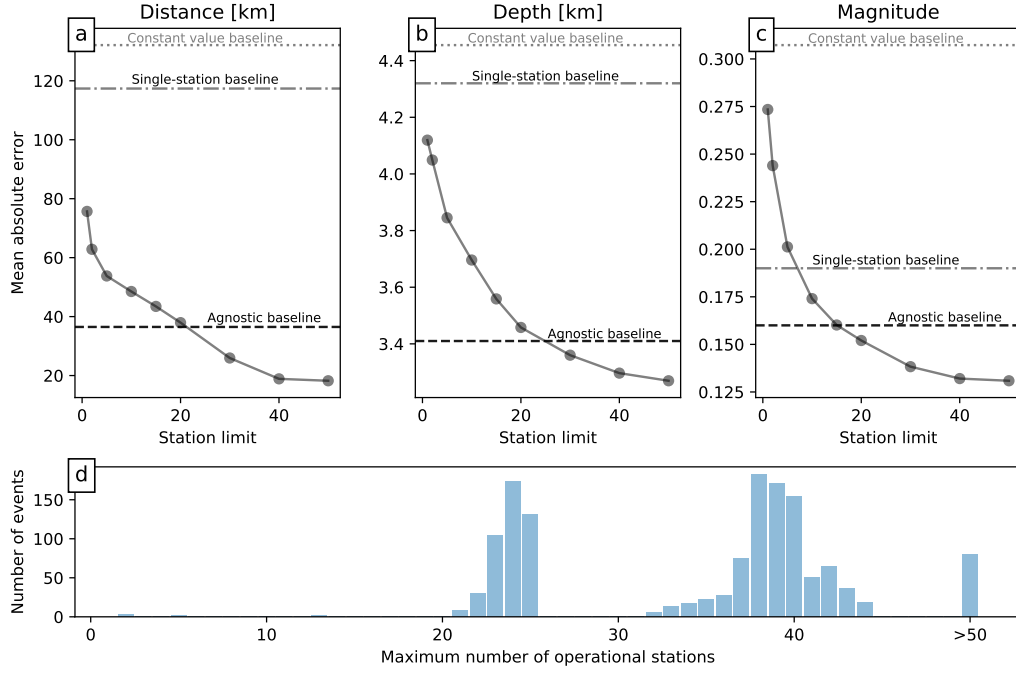


**Figure 3.** Effect of the number of available stations on the mean absolute error of the model predictions for (a) epicentral location, (b) hypocentral depth, and (c) event magnitude. When the number of stations included at inference time is increased, the misfit between the model predictions and the catalogue values decreases. The horizontal dashed and/or dotted lines in the top panels represents the baselines discussed in the text. Panel (d) displays the frequency distribution of the number of stations recording a given event.

274 may encode epicentral distance information. Combined with the amplitude of the wave-  
 275 forms, this may implicitly encode magnitude information.

276 Related to this, we investigate the effect of the (maximum) number of stations in-  
 277 cluded at inference time by selecting, for each event, the stations recording the waveforms  
 278 with the  $M$  highest standard deviations. All other waveforms are set to zero and there-  
 279 fore do not contribute to the predictions. If a given event was recorded by fewer than  
 280  $M$  stations, only the maximum number of operational stations was used with no aug-  
 281 mentation. We perform the inference for  $M = \{1, 2, 5, 10, 15, 20, 30, 40, 50\}$  stations, and  
 282 compute the mean absolute error of the predictions for the epicentre location (expressed  
 283 as a distance in km; Fig. 3a), hypocentral depth (Fig. 3b), and event magnitude (Fig. 3c).  
 284 For all the predicted quantities, we observe that the misfit with the catalogue values rapidly

285 decreases with the maximum number of stations included in the analysis, until the per-  
 286 formance saturates at around  $M \geq 40$ . The reason for this saturation may lie in the  
 287 distribution of the number of operational stations per event (Fig. 3d). Since the major-  
 288 ity of catalogued events is recorded by fewer than 40 stations, increasing  $M$  beyond 40  
 289 is only potentially beneficial only for a small number of events. For reference, we com-  
 290 pute two performance baselines: firstly, we take the mean value of each quantity (lat-  
 291 itude, longitude, depth, magnitude) over the catalogue and calculate the mean absolute  
 292 error relative to these. This baseline represents the performance of a “biased coin flip”  
 293 (i.e. random guessing). Secondly, we train our model specifically using only a single sta-  
 294 tion per training sample, through which the method specialises to single-waveform anal-  
 295 ysis (c.f. Perol et al., 2018; Lomax et al., 2019; Mousavi & Beroza, 2020). These base-  
 296 lines are included in Fig. 3 as horizontal dotted and dashed-dotted lines for the mean  
 297 absolute error relative to the (constant value) mean, and for the single-station model,  
 298 respectively. Strikingly, the model that was trained on the single-station waveforms achieves  
 299 worse performance in terms of the predicted hypocentre locations than the model trained  
 300 on 50 stations, but using only a single station at inference time. A possible explanation  
 301 for this, is that the single-station model may have gotten attracted to a poor local min-  
 302 imum in the loss landscape, after which the model started over-fitting, whereas the 50-  
 303 station model was able to generalise better and descended into a better local minimum.

304 Lastly, we compare our model performance with a model that treats the seismic  
 305 network as an Euclidean object, and hence has no explicit knowledge of the geographic  
 306 locations of the seismic stations (“station-location agnostic”). This station-location ag-  
 307 nostic model only features components #1 and #3 (see Fig. 1 and Supplementary Text  
 308 S2 for details) and does not incorporate the station locations among the data features.  
 309 Instead, the stations appear in a fixed order in a grid-like arrangement of size  $N_s \times N_t \times$   
 310 3, where  $N_s = 256$  denotes the total number of stations in the network (187) plus zero  
 311 padding to make  $N_s$  an integer power of two. Potentially, the station-location agnostic  
 312 model is able to “learn” the configuration of the seismic network and implicitly utilise  
 313 station locations in predicting the seismic source characteristics. As in most traditional  
 314 CNN approaches, we use a 2D kernel of size  $k_s \times k_t$  with  $k_s = 3$  so that information  
 315 from “neighbouring” stations (i.e. sequentially appearing in the grid, which does not im-  
 316 ply geographic proximity) is combined into the next layer of the model. Downsampling  
 317 of the data is performed along both the temporal and station axes. Even though the num-

318 ber of free parameters of the station-location agnostic model is almost twice that of the  
319 graph-based model (owing to the larger convolutional kernels), and even though the model  
320 has access to all the stations simultaneously, the prediction error of the seismic source  
321 parameters is significantly larger (dashed line in Fig. 3). Moreover, the station-location  
322 agnostic model required 5 times more computation time per training epoch. Hence, the  
323 GNN approach proposed here offers substantial benefits in terms of predictive power and  
324 ease of training.

### 325 **3.3 Potential applications**

326 The method proposed in this study does not require the intervention of an analyst  
327 to prepare or verify the model input data (e.g. picking P- and S-wave first arrivals), and  
328 so it can operate autonomously. This, combined with the rapid inference time of  $\approx 3.5$  ms  
329 for 50 stations, opens up applications in automated source characterisation that require  
330 a rapid response, such as earthquake early warning (EEW; Allen & Melgar, 2019), emer-  
331 gency response, and timely public dissemination. The aim of this study is to demonstrate  
332 the potential of incorporating seismic station locations (and possibly other node or edge  
333 attributes in a graph structure). Therefore, the model architecture was not optimised  
334 with the purpose of EEW in mind. Nonetheless, its modular nature allows for modifi-  
335 cations required to accommodate the real-time demands of EEW.

336 The first out of three components of this model consists of a CNN that analyses  
337 the waveforms of each seismic station and yields a set of station-specific features. The  
338 advantage of using a CNN is that it has immediate access to all the available informa-  
339 tion to produce a set of features optimal for the subsequent MLP components. Alter-  
340 natively, a different class of deep neural networks, the Recurrent Neural Networks (RNN;  
341 Hochreiter & Schmidhuber, 1997; Sherstinsky, 2020), allows for online (real-time) pro-  
342 cessing of time series. Within the generalised framework of GNNs (Battaglia et al., 2018),  
343 replacing the first CNN component with an RNN produces an equally valid model ar-  
344 chitecture, still independent of the number and ordering of stations. Hence, the proposed  
345 graph architecture can be adapted to meet demands of real-time processing for EEW.  
346 Flexibility in the number of stations included in the model input facilitates processing  
347 of an expanding data set as more seismic stations experience ground shaking after the  
348 first detection. For the applications of emergency response and information dissemina-

349 tion, the real-time requirements are less stringent, so that some response time may be  
350 sacrificed in favour of prediction accuracy.

351 Our method can be readily applied to automated earthquake catalogue generation  
352 in regions where large volumes of raw data exist, but which have not been fully processed.  
353 This typically arises in aftershock campaigns with stations that were not telemetered,  
354 for instance Ocean Bottom Seismometers. Given the relatively small size of the GNN  
355 employed here, re-training a pre-trained model on data from a different region is rela-  
356 tively inexpensive. Out of the 110,836 trainable parameters, less than half (42,244) re-  
357 side in the second and third components of the network. The first CNN component is  
358 completely agnostic to any spatial or regional information, as it only extracts features  
359 from time series of individual stations. Hence, if the waveforms in the target region are  
360 similar to those in the initial training region, the first component requires no re-training.  
361 This leaves only the smaller second and third MLP components to be re-trained and adapted  
362 to the characteristics of the target region. As such, fewer training seismic events than  
363 employed for the initial training will be required for fine-tuning of the model. With the  
364 re-trained model, the predicted hypocentre locations yield approximate phase arrival times  
365 at the various stations in the seismic network, which serve as a basis to set the windows  
366 for cross-correlation time-delay estimation and subsequent double-difference relocation.

367 Lastly, we point out that the GNN-approach laid out in this work is rather gener-  
368 al, and may be adapted to other applications, such as seismic event detection or clas-  
369 sification, that benefit from geographic or relational information of the seismic network.  
370 In cases where e.g. inter-station distance is relevant, additional architectural components  
371 can be considered (following the framework defined by Battaglia et al., 2018).

## 372 4 Conclusions

373 In this study we propose a method to incorporate the geometry of a seismic net-  
374 work into deep learning architectures using a Graph Neural Network (GNN) approach,  
375 applied to the task of seismic source characterisation (earthquake location and magni-  
376 tude estimation). By incorporating the geographic location of stations into the learn-  
377 ing and prediction process, we find that the deep learning model achieves superior per-  
378 formance in predicting the seismic source characteristics (epicentral latitude/longitude,  
379 hypocentral depth, and event magnitude) compared to a model that is agnostic to the

380 layout of the seismic network. In this way, multi-station waveforms can be incorporated  
381 while preserving flexibility to the number of available seismic stations, and invariance  
382 to the ordering of the station recordings. The GNN-based approach warrants the explo-  
383 ration of new avenues in earthquake early warning and rapid earthquake information,  
384 as well as in automated earthquake catalogue generation or other seismological tasks.

385

## 386 **Acknowledgements**

### 387 **Acknowledgments**

388 MvdE is supported by French government through the UCA<sup>JEDI</sup> Investments in the Fu-  
389 ture project managed by the National Research Agency (ANR) with the reference num-  
390 ber ANR-15-IDEX-01. The authors acknowledge computational resources provided by  
391 the ANR JCJC E-POST project (ANR-14-CE03-0002-01JCJC E-POST). Python codes  
392 and the pre-trained model are available from: <https://doi.org/10.6084/m9.figshare.12231077>  
393 [currently available at: <https://figshare.com/s/90000bfc549e3e688057>]



394 **References**

- 395 Allen, R. M., & Melgar, D. (2019). Earthquake Early Warning: Advances, Scientific  
 396 Challenges, and Societal Needs. *Annual Review of Earth and Planetary Sciences*,  
 397 47(1), 361–388. (eprint: <https://doi.org/10.1146/annurev-earth-053018-060457>)  
 398 doi: 10.1146/annurev-earth-053018-060457
- 399 Battaglia, P. W., Hamrick, J. B., Bapst, V., Sanchez-Gonzalez, A., Zambaldi, V.,  
 400 Malinowski, M., . . . Pascanu, R. (2018, October). Relational inductive biases,  
 401 deep learning, and graph networks. *arXiv:1806.01261 [cs, stat]*.
- 402 Beyreuther, M., Barsch, R., Krischer, L., Megies, T., Behr, Y., & Wassermann, J.  
 403 (2010, May). ObsPy: A Python Toolbox for Seismology. *Seismological Research*  
 404 *Letters*, 81(3), 530–533. doi: 10.1785/gssrl.81.3.530
- 405 Bronstein, M. M., Bruna, J., LeCun, Y., Szlam, A., & Vandergheynst, P. (2017,  
 406 July). Geometric Deep Learning: Going beyond Euclidean data. *IEEE Signal*  
 407 *Processing Magazine*, 34(4), 18–42. doi: 10.1109/MSP.2017.2693418
- 408 Cui, Z., Henrickson, K., Ke, R., & Wang, Y. (2019). Traffic Graph Convolutional  
 409 Recurrent Neural Network: A Deep Learning Framework for Network-Scale Traf-  
 410 fic Learning and Forecasting. *IEEE Transactions on Intelligent Transportation*  
 411 *Systems*, 1–12. doi: 10.1109/TITS.2019.2950416
- 412 Duvenaud, D. K., Maclaurin, D., Iparraguirre, J., Bombarell, R., Hirzel, T., Aspuru-  
 413 Guzik, A., & Adams, R. P. (2015). Convolutional Networks on Graphs for  
 414 Learning Molecular Fingerprints. In C. Cortes, N. D. Lawrence, D. D. Lee,  
 415 M. Sugiyama, & R. Garnett (Eds.), *Advances in Neural Information Processing*  
 416 *Systems 28* (pp. 2224–2232). Curran Associates, Inc.
- 417 Dysart, P. S., & Pulli, J. J. (1990, December). Regional seismic event classification  
 418 at the NORESS array: Seismological measurements and the use of trained neural  
 419 networks. *Bulletin of the Seismological Society of America*, 80(6B), 1910–1933.
- 420 Gal, Y., & Ghahramani, Z. (2016). Dropout as a Bayesian Approximation: Repre-  
 421 senting Model Uncertainty in Deep Learning. *Proceedings of the 33rd International*  
 422 *Conference on International Conference on Machine Learning*, 48, 1050–1059.
- 423 Gilmer, J., Schoenholz, S. S., Riley, P. F., Vinyals, O., & Dahl, G. E. (2017, June).  
 424 Neural Message Passing for Quantum Chemistry. *Proceedings of the 34th Interna-*  
 425 *tional Conference on Machine Learning*, 70, 1263–1272.
- 426 Gori, M., Monfardini, G., & Scarselli, F. (2005, July). A new model for learn-

- 427 ing in graph domains. In *Proceedings. 2005 IEEE International Joint Con-*  
428 *ference on Neural Networks, 2005.* (Vol. 2, p. 729-734 vol. 2). doi: 10.1109/  
429 IJCNN.2005.1555942
- 430 Hamilton, W. L., Ying, R., & Leskovec, J. (2017, December). Inductive representa-  
431 tion learning on large graphs. In *Proceedings of the 31st International Conference*  
432 *on Neural Information Processing Systems* (pp. 1025–1035). Long Beach, Califor-  
433 nia, USA: Curran Associates Inc.
- 434 Hochreiter, S., & Schmidhuber, J. (1997, November). *Long Short-Term Memory.*  
435 MIT Press.
- 436 Hu, W., Xiao, L., & Pennington, J. (2020, January). Provable Benefit of Orthogonal  
437 Initialization in Optimizing Deep Linear Networks. *arXiv:2001.05992 [cs, math,*  
438 *stat]*.
- 439 Hutton, K., Woessner, J., & Hauksson, E. (2010, April). Earthquake Monitoring in  
440 Southern California for Seventy-Seven Years (1932–2008). *Bulletin of the Seismo-*  
441 *logical Society of America*, 100(2), 423–446. doi: 10.1785/0120090130
- 442 Kingma, D. P., & Ba, J. (2017, January). Adam: A Method for Stochastic Opti-  
443 mization. *arXiv:1412.6980 [cs]*.
- 444 Kriegerowski, M., Petersen, G. M., Vasyura-Bathke, H., & Ohrnberger, M. (2019,  
445 March). A Deep Convolutional Neural Network for Localization of Clustered  
446 Earthquakes Based on Multistation Full Waveforms. *Seismological Research Let-*  
447 *ters*, 90(2A), 510–516. doi: 10.1785/0220180320
- 448 Li, Z., Meier, M.-A., Hauksson, E., Zhan, Z., & Andrews, J. (2018). Ma-  
449 chine Learning Seismic Wave Discrimination: Application to Earthquake  
450 Early Warning. *Geophysical Research Letters*, 45(10), 4773–4779. (\_eprint:  
451 <https://agupubs.onlinelibrary.wiley.com/doi/pdf/10.1029/2018GL077870>) doi:  
452 10.1029/2018GL077870
- 453 Lomax, A., Michelini, A., & Jozinović, D. (2019, March). An Investigation of Rapid  
454 Earthquake Characterization Using Single-Station Waveforms and a Convolu-  
455 tional Neural Network. *Seismological Research Letters*, 90(2A), 517–529. doi:  
456 10.1785/0220180311
- 457 Madariaga, R. (1976). Dynamics of an expanding circular fault. *Bull. Seismol. Soc.*  
458 *Am*, 639–666.
- 459 Monti, F., Boscaini, D., Masci, J., Rodolà, E., Svoboda, J., & Bronstein, M. M.

- 460 (2017, July). Geometric Deep Learning on Graphs and Manifolds Using Mix-  
 461 ture Model CNNs. In *2017 IEEE Conference on Computer Vision and Pattern  
 462 Recognition (CVPR)* (pp. 5425–5434). doi: 10.1109/CVPR.2017.576
- 463 Mousavi, S. M., & Beroza, G. C. (2020). A Machine-Learning  
 464 Approach for Earthquake Magnitude Estimation. *Geophys-  
 465 ical Research Letters*, *47*(1), e2019GL085976. (\_eprint:  
 466 <https://agupubs.onlinelibrary.wiley.com/doi/pdf/10.1029/2019GL085976>) doi:  
 467 10.1029/2019GL085976
- 468 Mousavi, S. M., Zhu, W., Sheng, Y., & Beroza, G. C. (2019, July). CRED: A Deep  
 469 Residual Network of Convolutional and Recurrent Units for Earthquake Signal  
 470 Detection. *Scientific Reports*, *9*(1), 1–14. doi: 10.1038/s41598-019-45748-1
- 471 Perol, T., Gharbi, M., & Denolle, M. (2018, February). Convolutional neural net-  
 472 work for earthquake detection and location. *Science Advances*, *4*(2), e1700578.  
 473 doi: 10.1126/sciadv.1700578
- 474 Powers, P. M., & Jordan, T. H. (2010). Distribution of  
 475 seismicity across strike-slip faults in California. *Journal  
 476 of Geophysical Research: Solid Earth*, *115*(B5). (\_eprint:  
 477 <https://agupubs.onlinelibrary.wiley.com/doi/pdf/10.1029/2008JB006234>) doi:  
 478 10.1029/2008JB006234
- 479 Qi, C. R., Yi, L., Su, H., & Guibas, L. J. (2017, December). PointNet++: Deep  
 480 hierarchical feature learning on point sets in a metric space. In *Proceedings of  
 481 the 31st International Conference on Neural Information Processing Systems* (pp.  
 482 5105–5114). Long Beach, California, USA: Curran Associates Inc.
- 483 Sanchez-Gonzalez, A., Bapst, V., Cranmer, K., & Battaglia, P. (2019, September).  
 484 Hamiltonian Graph Networks with ODE Integrators. *arXiv:1909.12790 [physics]*.
- 485 Saxe, A., McClelland, J. L., & Ganguli, S. (2014). Exact solutions to the nonlinear  
 486 dynamics of learning in deep linear neural networks. In *International Conference  
 487 on Learning Representations*.
- 488 Sherstinsky, A. (2020, March). Fundamentals of Recurrent Neural Network (RNN)  
 489 and Long Short-Term Memory (LSTM) network. *Physica D: Nonlinear Phenom-  
 490 ena*, *404*, 132306. doi: 10.1016/j.physd.2019.132306
- 491 Srivastava, N., Hinton, G., Krizhevsky, A., Sutskever, I., & Salakhutdinov, R.  
 492 (2014). Dropout: A simple way to prevent neural networks from overfitting.

- 493 *Journal of Machine Learning Research*, 15(56), 1929–1958.
- 494 Tompson, J., Goroshin, R., Jain, A., LeCun, Y., & Bregler, C. (2015, June). Ef-  
495 ficient object localization using Convolutional Networks. In *2015 IEEE Confer-*  
496 *ence on Computer Vision and Pattern Recognition (CVPR)* (pp. 648–656). doi:  
497 10.1109/CVPR.2015.7298664
- 498 Wang, Y., Sun, Y., Liu, Z., Sarma, S. E., Bronstein, M. M., & Solomon, J. M. (2019,  
499 October). *Dynamic Graph CNN for Learning on Point Clouds*. Association for  
500 Computing Machinery.
- 501 Wu, Y., Lin, Y., Zhou, Z., Bolton, D. C., Liu, J., & Johnson, P. (2019, January).  
502 DeepDetect: A Cascaded Region-Based Densely Connected Network for Seismic  
503 Event Detection. *IEEE Transactions on Geoscience and Remote Sensing*, 57(1),  
504 62–75. doi: 10.1109/TGRS.2018.2852302
- 505 Zhou, J., Cui, G., Zhang, Z., Yang, C., Liu, Z., Wang, L., . . . Sun, M. (2019,  
506 July). Graph Neural Networks: A Review of Methods and Applications.  
507 *arXiv:1812.08434 [cs, stat]*.